ChemComm

COMMUNICATION

View Article Online
View Journal | View Issue

Cite this: *Chem. Commun.*, 2020, **56**, 15220

Received 10th June 2020,
Accepted 6th November 2020

DOI: 10.1039/d0cc04061d

rsc.li/chemcomm

The range of antiferromagnetic coupling governs the conductivity: semiconducting behavior and ammonia gas sensing property of diamagnetic hexaradical-containing tetranuclear Co^{III}_4 cluster and its nonradical congener†‡

Prasenjit Sarkar, [a] Tukhar Jyoti Konch,[a] Tapas Kamilya,[b] Kalyan Raidongia, [a] Somobrata Acharya [b] and Chandan Mukherjee *[a]

Long-range antiferromagnetic coupling impeded electron flow through the hexaradical-containing tetranuclear Co^{III}_4 complex (1), while the nonradical-containing tetranuclear Co^{III}_4 complex (2), with no paramagnetic centres, was a semiconductor and sensed NH_3 efficiently at room temperature (25 °C).

Ammonia gas is a harmful pollutant, which is accumulating in the environment mainly as a result of industrial and agricultural activities, decomposition of waste plants and dead animals, automotive emissions, and chemical combustion.[1] Exposure to ammonia gas with a concentration of more than 50 ppm causes skin and eye irritation, while exposure to higher levels, of 500 ppm, is life-threatening and causes fatal respiratory distress, including pulmonary oedema (fluid accumulation in the lungs).[1c] In the human body, ammonia is produced in about 0.1 ppm by natural enzymatic activities. The concentration increases to a level of about 2 ppm in cases of kidney disorder and stomach ulcers, through bacterial activity.[1c] Therefore, development of an ammonia gas sensor for quantification and monitoring of ammonia gas is imperative for the safety of human health and clinical diagnosis.

Over the past few decades, a lot of research on the development of ammonia gas sensors has been pursued using optical-, electrochemical-, and semiconductor-based materials.[2] Among these, semiconductor-based sensors are preferred due to their long lifetime, economical benignity, and operational feasibility under harsh conditions at low potentials. In this context, SnO_2, ZnO, WO_3, *etc.*, metal oxide-based semiconductors, are the most common and extensively used as gas sensors.[3] While the sensitivity of the oxides is good, their main drawbacks are poor selectivity, long response time, and high-temperature functionality. To deal with these issues, organic semiconductors,[4] nanostructured graphenes,[5] porphyrinoids and the corresponding metal complexes,[6] and metal-phthalocyanine-radical complexes[7] have been investigated extensively. In this study, we explore hexaradical- and nonradical-containing tetranuclear Co^{III}_4 complexes. The aim is twofold: (1) understanding the origin of conductivity in the materials, and (2) use of the conducting-material-based device as an NH_3 sensor at room temperature. In this regard, the non-innocent (redox-active) ligand $H_4L^{Se(AP)}$ and innocent salen congener, ligand $H_2L^{Se(Sal)}$, have been introduced (Scheme 1). Both the ligands were synthesized in good yields by condensation reactions of bis(2-aminophenyl)diselenide (**A**) with

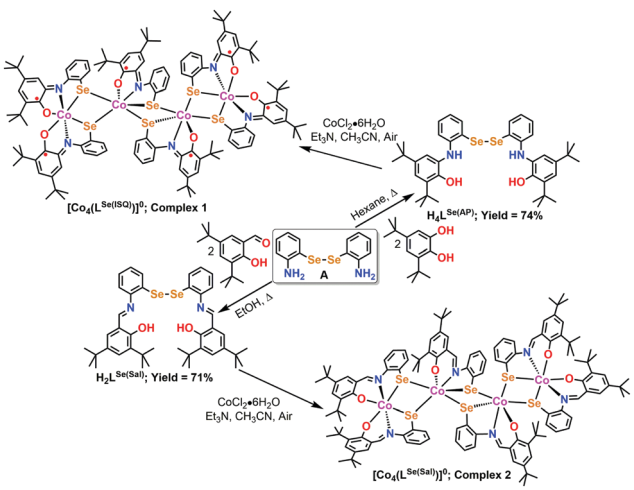

Scheme 1 Schematic representation for the synthesis of ligands and the corresponding Co(III) complexes.

[a] *Department of Chemistry, Indian Institute of Technology Guwahati, Assam-781039, India. E-mail: cmukherjee@iitg.ac.in*
[b] *School of Applied & Interdisciplinary Sciences, Indian Association for the Cultivation of Science, Jadavpur, Kolkata 700032, India*

† C. M. formulated the project and wrote the manuscript. P. S. synthesized and characterized the complexes. T. J. K. and K. R. pursued gas-sensing studies. P. S., T. K. and S. A. performed conductivity studies.

‡ Electronic supplementary information (ESI) available: Spectroscopic characterization spectra of the ligands and the complexes. Crystallographic, bond distances and bond angles tables for complex **1** and complex **2**. CCDC 2007091 and 2007097. For ESI and crystallographic data in CIF or other electronic format see DOI: 10.1039/d0cc04061d

either 3,5-di-*tert*-butylcatechol or 3,5-di-*tert*-butylsalicylaldehyde under refluxing conditions. The reaction of $CoCl_2{\cdot}6H_2O$ with 0.75 equivalent amounts of $H_4L^{Se(AP)}$/$H_2L^{Se(Sal)}$ ligand and Et_3N in CH_3CN in the presence of air provided complex **1**/complex **2** in 62%/46% yield (Scheme 1). Detailed procedures are given in the ESI.‡

Electrospray ionization (ESI)-mass spectra were recorded in the positive-ion mode for $H_4L^{Se(AP)}$, $H_2L^{Se(Sal)}$, complex **1**, and complex **2** in acetonitrile solutions. In the mass spectra of ligands $H_4L^{Se(AP)}$ $[C_{40}H_{52}N_2O_2Se_2]$ and $H_2L^{Se(Sal)}$ $[C_{42}H_{52}N_2O_2Se_2]$, a 100% molecular ion peak appeared at m/z = 753.25 amu and m/z = 777.25 amu, respectively. Investigation of the isotope distribution patterns revealed that the observed masses corresponded to the compositions $[C_{40}H_{52}N_2O_2Se_2 + H]^+$ and $[C_{42}H_{52}N_2O_2Se_2 + H]^+$, respectively (Fig. S2, ESI‡). Thus, formation of the expected ligands was supported. The molecular ion peaks at m/z = 2476.36 amu (100%), for complex **1**, and at m/z = 2555.72 amu (100%), for complex **2**, were consistent with the compositions $[Co_4(L^{Se(AP)})_3]^+$ and $[Co_4(L^{Se(Sal)})_3 + H]^+$, respectively (Fig. S8 and S9, ESI‡).

Complex **1** and complex **2** were structurally characterized by single-crystal X-ray diffraction measurements at 100 K. Both the complexes crystallized in the triclinic space group $P\bar{1}$. The molecular structures of complex **1** and complex **2** are almost identical (Fig. 1). Each structure comprised a tetranuclear Co_4 core that consists of four Co ions and six tridentate ligand units of the ONSe donor set. In each core, all the four Co ions were six-coordinate. While the coordination sites of the two terminal Co ions were occupied by two ONSe donor sets in meridional fashion, the interior Co ions were coordinated by one ONSe donor set and three bridging Se ions. The distances between the two proximal Se atoms in the complexes were in the range 3.17–3.27 Å. This indicated clearly that the diselane bond (Se–Se = 2.29 ± 0.01 Å), present in the diphenyldiselane backbones of the two ligands, was cleaved during the complexation.

In complex **1**, Co–O, Co–N, and Co–Se bond distances were within the ranges 1.914(3)–1.938(4) Å, 1.885(4)–1.914(4) Å, and 2.3269(8)–2.4196(8) Å, respectively (Table S1, ESI‡). The bond distances were commensurate with the previously reported low-spin Co(III) complexes with a similar ligand (2-amidophenolate) environment.[8] The C–Se bond distances were 1.904–1.933 Å, which corresponded to the $PhSe^-$ form, as in previous literature reports.[9] The C–C bond distances of the *tert*-butyl groups containing the C_6 ring in each ligand unit were unequal. A quinoidal-type distortion, *i.e.*, a systematic short-long-short bond sequence, followed by three long bonds, was noticed

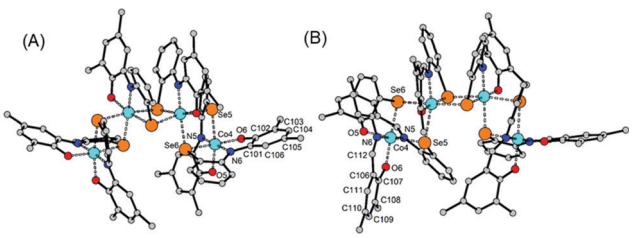

Fig. 1 Molecular structures of: (A) complex **1**, and (B) complex **2**. H atoms and methyl groups attached to *tert*-butyl C atoms are omitted for clarity.

Table 1 Selected bond distances (Å) of complex **1** and complex **2**

Bonds	Complex **1**	Bonds	Complex **2**
Co4–Se5	2.3382(8)		2.4016(8)
Co4–Se6	2.3349(8)		2.3083(8)
Co4–N5	1.889(4)		1.923(4)
Co4–N6	1.899(4)		1.931(4)
Co4–O5	1.928(3)		1.925(3)
Co4–O6	1.926(3)		1.918(3)
C101–C102	1.440(7)	C106–C107	1.450(7)
C101–C106	1.410(7)	C107–C108	1.455(7)
C102–C103	1.424(7)	C108–C109	1.353(8)
C103–C104	1.384(7)	C109–C110	1.430(8)
C104–C105	1.411(8)	C110–C111	1.358(8)
C105–C106	1.352(7)	C106–C111	1.413(7)
C101–N6	1.364(6)	C106–C112	1.410(7)
C102–O6	1.316(5)	C112–N6	1.303(6)
		C107–O6	1.286(6)

(Table 1). This type of distortion has previously been observed in the one-electron-oxidized, as well as the two-electron-oxidized, 2-amidophenolate units.[10] In the one-electron-oxidized iminosemiquinone form, C–O and C–N bond distances are in between that of the single bond (C–O = 1.35 Å and C–N = 1.37 Å) and the double bond (C–O = 1.24 Å and C–N = 1.30 Å) range. Herein, the average C–O = 1.307 Å and C–N = 1.361 Å thus referred to iminosemiquinone form of the coordinated 2-amidophenolate units. Hence, each tridentate ligand with ONSe donor set was dinegative with an iminosemiquinone radical, *i.e.* $(L^{Se(ISQ)})^{2-}$, and coordinated to low-spin Co(III) ions.

In complex **2**, the average Co–O and Co–N_{imine} (N_{imine} corresponds to the N atom belonging to an imine moiety) bond distances were 1.923 and 1.926 Å, respectively. The bond distances were in accord with the six-coordinate low-spin Co(III)-salen complexes reported in the literature.[11] Hence, the spin state and the oxidation state of the Co ions have been assigned as low-spin and +III. In uncoordinated salen ligands, phenolic C–O and imine C–N bond distances generally appear at about 1.35 Å and 1.28 Å, respectively. In complex **2**, the average distances C–O = 1.302 Å and C–N = 1.302 Å were observed. The shortening of the phenolic bonds and elongation of the corresponding imine C–N bonds indicated clearly that the mononegative charge on the phenolic O atoms was being delocalized up to the imine N atoms through the phenyl ring system.[11a] The C–Se bond distances (1.892–1.933 Å) in complex **2** were similar to those in complex **1**. Therefore, each coordinating tridentate ligand in complex **2** acquired a 2^- formal charge. Thus, the composition of the neutral complex was four low-spin Co(III) ions and six $(L^{Se(Sal)})^{2-}$ ligands.

Complex **1** consisted of six ligand-based unpaired electrons, *i.e.*, iminosemiquinone radicals (*vide supra*, molecular structure analysis) with an S_R = 1/2 spin for each radical. Variable-temperature magnetic susceptibility measurement on complex **1** referred to the diamagnetic character in the entire temperature range of 2–300 K (Fig. S14, ESI‡). Thus, strong antiferromagnetic coupling interactions amongst the paramagnetic centers prevailed. Complex **2** comprised low-spin Co(III) ions ($S_{Co(III)}$ = 0, $3d^6$) and no ligand-based radicals. Hence, it was diamagnetic. The ^1H NMR spectrum was congruent with the diamagnetic nature of the complex.

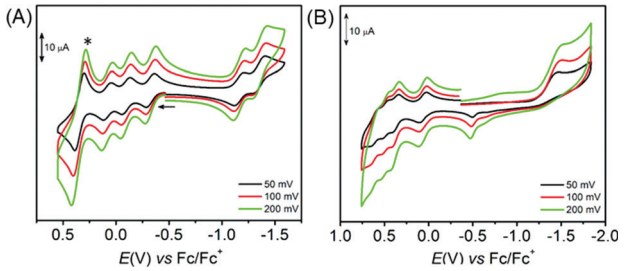

Fig. 2 Cyclic voltammograms of: (A) complex **1** and (B) complex **2** measured at 50, 100, and 200 mV. *Indicates the two-electron process.

Cyclic voltammograms (CVs) of complex **1** (+0.55 to −1.60 V) and complex **2** (+0.75 to −1.85 V) were recorded in CH_2Cl_2 at various scan rates (Fig. 2). The CV of complex **1** displayed four reversible oxidation waves and two reversible reduction waves. The oxidations at $E^{ox}_{1/2}$ = −0.323, −0.090, and +0.087 V were single-electron processes, while the oxidation at $E^{ox}_{1/2}$ = ∼+0.347 V corresponded to a two-electron process. The peak separation of the two-electron oxidation process was scan-rate dependent; at higher scan rate (200 mV s^{-1}) the peak separation was 0.133 V, while the separation was 0.086 V at a scan rate of 50 mV s^{-1}. This feature emphasized that two one-electron oxidations happened almost at the same potential. Two one-electron reductions occurred at $E^{Red}_{1/2}$ = −1.153 and −1.360 V. The oxidation and reduction potential windows were comparable to the previously reported low-spin Co(III)-tris(iminosemiquinone) complex of the *N*-phenyl-3,5-di-*tert*-butyl-2-aminophenol ligand, where the oxidation and reduction processes are ligand centered, *i.e.*, oxidations lead to iminoquinone formation and reductions generate amidophenolate units.[12] Hence, here the redox processes were also assigned as ligand centered. In complex **2**, four reversible one-electron oxidations occurred at $E^{ox}_{1/2}$ = +0.058, +0.373, +0.498 and +0.608 V. In the complex, oxidations led to the formation of phenoxyl radicals from phenolate units.[11a] The reduction that appeared at E^{Red} = −1.478 V was irreversible in nature and possibly referred to the reduction of a Co(III) ion to a Co(II) ion.

The current–voltage characteristics for thin films of complex **1** and complex **2** were investigated (Fig. 3A) by using a TTPx Lakeshore probe station and a semiconductor characterization system (Keithley 4200 SCS) under vacuum conditions to ensure the absence of external effects on the current from gas and dust particles. Complex **1** behaved as an insulator, since a low current (maximum 15 nA) was realized across a ±10 V bias (Fig. 3B). The corresponding conductivity, $\sigma = 1.34 \times 10^{-7}$ S cm^{-1}, was also low at 1 V. However, complex **2** showed a high current of 58 μA at 10 V with a conductivity of $\sigma = 5.43 \times 10^{-5}$ S cm^{-1} at 1 V (Fig. 3C). The non-linear nature of the *I–V* curve (Fig. 3C) and the decrease in resistance with increasing temperature (Fig. S25, ESI‡) indicated that complex **2** was a semiconductor. Thus, the adverse conducting nature between the two diamagnetic [$S_T(\mathbf{1}) = 0$, $S_T(\mathbf{2}) = 0$] complexes has demonstrated the effect of long-range antiferromagnetic coupling among the six S_R = 1/2 spins of the six radicals in complex **1**. The unpaired electrons with opposite spins impeded the electron flow in complex **1**, possibly due to high

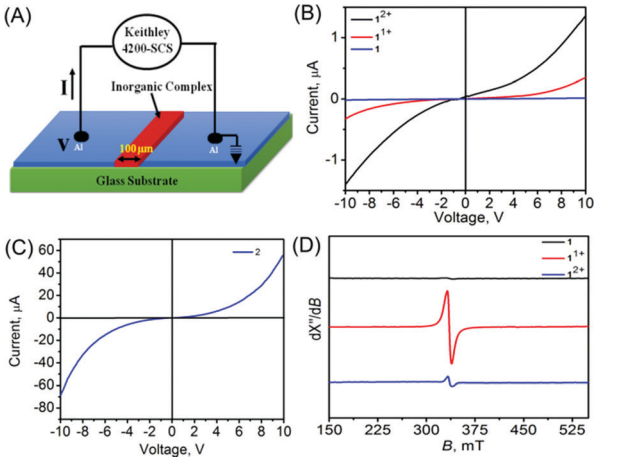

Fig. 3 (A) Pictorial representation of *I–V* measurement set-up. *I–V* characteristic plots of: (B) complex **1**, $\mathbf{1}^{1+}$, and $\mathbf{1}^{2+}$; (C) complex **2**. (D) X-band EPR spectra of complex **1**, $\mathbf{1}^{1+}$ and $\mathbf{1}^{2+}$.

spin-exchange energy and/or electron deflection. Upon one-electron oxidation of complex **1**, a paramagnetic species ($\mathbf{1}^{1+}$) with an unpaired electron [$S_T(\mathbf{1}^{1+}) = 1/2$] resulted, as evidenced by the X-band EPR spectrum analysis (Fig. 3D). The species showed better conductivity, with $\sigma = 1.26 \times 10^{-6}$ S cm^{-1} at 1 V, compared to complex **1** (Fig. 3B). In this case, a long-range spin-frustrated system with total spin of S_T = 1/2 resulted (Fig. 4) and the conductivity materialized because of spin-polarization and spin-delocalization. Further oxidation of $\mathbf{1}^{1+}$ by an electron provided a diamagnetic species ($\mathbf{1}^{2+}$), as indicated by the X-band EPR spectrum study (Fig. 3D). *I–V* characteristics of the species showed much better semiconducting properties than **1** and $\mathbf{1}^{1+}$ (Fig. 3B). Thus, the increase in the conductivity ($\sigma = 8.85 \times 10^{-6}$ S cm^{-1} at 1 V) was due to the elimination of an antiferromagnetic coupling interaction between two S_R = 1/2 spins and the resultant shrinking of the antiferromagnetic coupling range (Fig. 4). It should be noted that the diamagnetic complex **2** was a better conductor compared to complex **1**. Hence, it is shown that the conductivity of the material is governed by the lack of antiferromagnetic coupling interactions.

Complex **2** was examined as an ammonia gas sensor at room temperature. In this context, the material was prepared by blending complex **2** with polytetrafluoroethylene. It was then placed between two Cu electrodes on a supporting glass plate (1 cm × 1 cm). The detailed procedure is given in the ESI.‡ Upon exposure to different concentrations (50–250 ppm) of ammonia gas (NH_3), the conductivity of the semiconducting

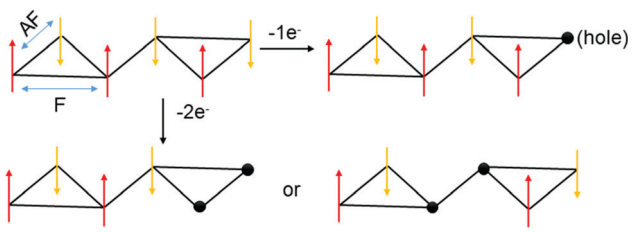

Fig. 4 Schematic representations of coupling schemes in **1**, $\mathbf{1}^{1+}$ and $\mathbf{1}^{2+}$ species. AF = antiferromagnetic coupling; F = ferromagnetic coupling.

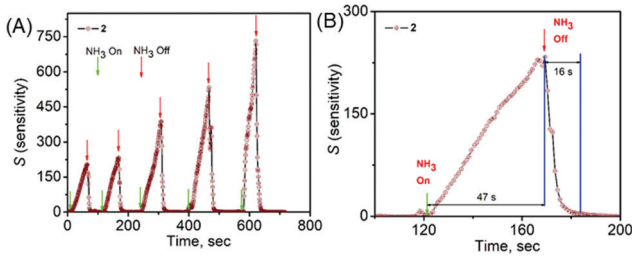

Fig. 5 (A) Sensing activity of complex **2** at different concentrations (in ppm) of NH_3 gas (50, 100, 150, 200 and 250 ppm) under an applied potential difference of 0.5 V. (B) Response and recovery times at 100 ppm concentration of NH_3 gas.

material, which was n-type as evidenced by the Mott–Schottky plot (Fig. S27, ESI‡), increased. The presence of the gas raises the electron density in the conduction band due to oxidation of NH_3 to N_2 by chemisorbed O_2^- ion,[13] and, therefore, the conductivity increases (Fig. S28, ESI‡). The relative sensing response ($S = I_{Ammonia} - I_{Air}/I_{Air}$) to NH_3 varied with the concentration (Fig. 5A). At 50 ppm, S = 205, and this increased to 732 at 250 ppm. The increase was almost proportional to the concentration of NH_3 (Fig. S31, ESI‡). The response–recovery behaviour for the sensing activity is depicted in Fig. 5B. For measurement concentrations of NH_3 of 50 to 250 ppm, the response time was within 40–60 s, and the recovery time was 10–17 s. These values are very much lower than those previously reported for many semiconductor-based NH_3 gas sensors that operate at room temperature. For instance, >200 s and >800 s have been reported as the respective response and recovery times for sensing of 100 ppm NH_3 at room temperature by a Co_3O_4-based nanosheet array.[13] $Cu_3(HHTP)_2$ thin film (HHTP = 2,3,6,7,10,11-hexahydroxytriphenylene) requires 82 s to respond to 100 ppm NH_3 gas and 547 s for recovery.[14] Hydroquinone-incorporated Mg-metal–organic framework was reported to respond to 50 ppm NH_3 in 87 s and to recover in 127s.[15]

The stability of complex **2** in the presence of NH_3 was demonstrated by examining the reproducibility of the sensing activity. In this regard, the material was initially exposed to 150 ppm NH_3 gas and then the gas was taken out. The relative sensing response was calculated for five successive cycles. No apparent change (Fig. S22, ESI‡) in the relative sensing response was noticed.

In summary, two tetranuclear low-spin Co^{III}_4 complexes with non-innocent ligand $H_4L^{Se(AP)}$ and innocent salen congener ligand $H_2L^{Se(Sal)}$ were successfully synthesized and characterized. Complex **1**, consisting of six radicals, was a diamagnetic material and an electric insulator. The successive oxidation of the complex by two one-electron processes bestowed semiconducting character on the resulting species. The shortening in the antiferromagnetic coupling range by the sequential removal of two electrons was responsible for the alteration. The diamagnetic complex **2** exhibited semiconducting behavior and successfully detected NH_3 gas at room temperature with the theoretical limit of detection of 5.04 ppm. The impressive response and recovery times, and reproducibility and durability, identified complex **2** as a useful sensor material. Further study on catalytic applications of the complexes will follow.

This project is funded by BT/PR23622/NNT/281294/2017 (DBT) and CRG/2020/000216 (SERB). P. S., T. J. K., and T. K. thank IIT Guwahati and UGC for their doctoral fellowships. C. M. is indebted to Prof. Mohd. Qureshi for his support. S. A. acknowledges CRG/2019/003907 (SERB).

Conflicts of interest

There are no conflicts to declare.

Notes and references

1 (*a*) S. Yamulki, R. M. Harrison and K. W. T. Goulding, *Atmos. Environ.*, 1996, **30**, 109; (*b*) R. K. Gangopadhyay and S. K. Das, *Process Saf. Prog.*, 2008, **27**, 15; (*c*) B. Timmer, W. Olthuis and A. von der Berg, *Sens. Actuators, B*, 2005, **107**, 666.
2 (*a*) S. Kempahanumakkagari, K. Vellingiri, A. Deep, E. E. Kwon, N. Bolan and Ki-H Kim, *Coord. Chem. Rev.*, 2018, **357**, 105; (*b*) A. Dey, *Mater. Sci. Eng., B*, 2018, **229**, 206; (*c*) F. Sassa, G. C. Biswas and H. Suzuki, *Lab Chip*, 2020, **20**, 1358.
3 (*a*) L. Zhu and W. Zeng, *Sens. Actuators, A*, 2017, **267**, 242; (*b*) C. S. Rout, M. Hegde, A. Govindaraj and C. N. R. Rao, *Nanotechnology*, 2007, **18**, 1; (*c*) D. Wong, O. Abuzalat, S. Mostafa, S. Park and S. Kim, *J. Mater. Chem. C*, 2020, **8**, 7567; (*d*) C. N. Xu, N. Miura, Y. Ishida, K. Matsuda and N. Yamazoe, *Sens. Actuators, B*, 2000, **65**, 163.
4 (*a*) C. Kumar, G. Rawat, H. Kumar, Y. Kumar, R. Prakash and S. Jit, *Sens. Actuators, B*, 2018, **225**, 203; (*b*) H. Zhang, H. Dong, Y. Li, W. Jiang, Y. Zhen, L. Jiang, Z. Wang, W. Chen, A. Wittmann and W. Hu, *Adv. Mater.*, 2016, **28**, 7466.
5 (*a*) D. W. Hatchett and M. Josowicz, *Chem. Rev.*, 2008, **108**, 746; (*b*) I.-P. Liu, C.-H. Chang and B.-Y. Ke, *ACS Appl. Electron. Mater.*, 2019, **8**, 1474.
6 (*a*) R. Paolesse, S. Nardis, D. Monti, M. Stefanelli and C. D. Natale, *Chem. Rev.*, 2017, **117**, 2517; (*b*) C. Wäckerlin, K. Tarafder, J. Girovsky, J. Nowakowski, T. Hählen, A. Shchyrba, D. Siewert, A. Kleibert, F. Nolting, P. M. Oppeneer, T. A. Jung and N. Ballav, *Angew. Chem., Int. Ed.*, 2013, **52**, 4568.
7 (*a*) K. P. Kamloth, Semiconductor Junction Gas Sensors, *Chem. Rev.*, 2008, **108**, 367; (*b*) O. A. Melville, T. M. Grant and B. H. Lessard, *J. Mater. Chem. C*, 2018, **6**, 5482.
8 P. Chaudhuri, R. Wagner, U. Pieper, B. Biswas and T. Weyhermüller, *Dalton Trans.*, 2008, 1286.
9 As an example: G. C. Paul, S. Ghorai and C. Mukherjee, *Chem. Commun.*, 2017, **53**, 8022.
10 (*a*) S. N. Brown, *Inorg. Chem.*, 2012, **51**, 1251; (*b*) P. Sarkar, A. Tiwari, A. Sarmah, S. Bhandary, R. K. Roy and C. Mukherjee, *Chem. Commun.*, 2016, **52**, 10613.
11 (*a*) N. Roy, S. Sproules, E. Bothe, T. Weyhermüller and K. Wieghardt, *Eur. J. Inorg. Chem.*, 2009, 2655; (*b*) S. Thakurta, R. J. Butcher, G. Pilet and S. Mitra, *J. Mol. Struct.*, 2009, **929**, 112.
12 H. Chun, C. N. Verani, P. Chaudhuri, E. Bothe, E. Bill, T. Weyhermüller and K. Wieghardt, *Inorg. Chem.*, 2001, **40**, 4157.
13 Z. Li, Z. Lin, N. Wang, J. Wang, W. Liu, K. Sun, Y. Q. Fu and Z. Wang, *Sens. Actuators, B*, 2016, **235**, 222.
14 M.-S. Yao, X.-J. Lv, Z.-H. Fu, W.-H. Li, W.-H. Deng, G. D. Wu and G. Xu, *Angew. Chem., Int. Ed.*, 2017, **56**, 16510.
15 Y.-P. Li, S.-N. Li, Y.-C. Jiang, M.-C. Hua and Q.-G. Zhai, *Chem. Commun.*, 2018, **54**, 9789.